
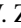





## Lowest-energy broad $\alpha$ -cluster resonances in $^{19}\text{F}$

A. Volya <sup>1,2,\*</sup>, V. Z. Goldberg <sup>2</sup>, A. K. Nurmukhanbetova <sup>3</sup>, D. K. Nauruzbayev <sup>4,5</sup> and G. V. Rogachev <sup>2,6,7</sup>

<sup>1</sup>*Department of Physics, Florida State University, Tallahassee 32306-4350, USA*

<sup>2</sup>*Cyclotron Institute, Texas A&M University, College Station, Texas 77843-3366, USA*

<sup>3</sup>*Energetic Cosmos Laboratory, Nazarbayev University, Nur-Sultan 010000, Kazakhstan*

<sup>4</sup>*Nazarbayev University Research and Innovation System, Nur-Sultan 010000, Kazakhstan*

<sup>5</sup>*Saint Petersburg State University, Saint Petersburg 199034, Russia*

<sup>6</sup>*Department of Physics and Astronomy, Texas A&M University, College Station, Texas 77843, USA*

<sup>7</sup>*Nuclear Solutions Institute, Texas A&M University, College Station, Texas 77843, USA*



(Received 26 April 2021; revised 17 September 2021; accepted 12 November 2021; published 18 January 2022)

There is a deep astrophysical interest in the structure of  $^{19}\text{F}$  states close to the  $\alpha$ -decay threshold. The nuclear structure of these states is important for understanding of the development of  $\alpha$  clustering in the  $^{20}\text{Ne}$  region. Emergence of clustered states, and generally states that favor coupling to reaction channels near the corresponding decay thresholds, is currently of special interest in theoretical physics. We specify the parameters of broad low spin states in  $^{19}\text{F}$  near the  $\alpha$ -decay threshold and present a theoretical study of these states. The study is limited to  $\ell = 0$  and 1 relative partial wave resonances in the  $\alpha + ^{15}\text{N}$  interaction close to the  $\alpha$ -decay threshold in  $^{19}\text{F}$ . Excitation function for  $^{15}\text{N}(\alpha, \alpha)$  elastic scattering was measured by the TTIK method. These new data together with the old, high-energy resolution data, were analyzed using the  $R$  matrix approach.  $^{19}\text{F}$  nuclear structure was calculated using configuration interaction methods with the recently developed effective interaction Hamiltonian. As a result, in this work we identify a series of  $\alpha$  clustering resonances in  $^{19}\text{F}$  and assess the distribution of the clustering strength, which is of importance to questions of astrophysics and for theoretical understanding of many-body physics and emergence of clustering in loosely bound or unstable nuclei. Progress has been made in theoretical understanding of the origins of clustering and questions for future theoretical and experimental research are identified.

DOI: [10.1103/PhysRevC.105.014614](https://doi.org/10.1103/PhysRevC.105.014614)

### I. INTRODUCTION

Fluorine is an element with an uncertain and widely debated cosmic origin. It has only one stable isotope,  $^{19}\text{F}$ , whose production and destruction is directly connected to the physical conditions in stars [1]. Asymptotic giant branch (AGB) stars, where  $^{19}\text{F}$  has been found via observations, are considered as an important source of  $^{19}\text{F}$  in the galaxy (see Ref. [2], and references therein). In AGB stars fluorine can be produced via reactions  $^{14}\text{N}(\alpha, \gamma)^{18}\text{F}(\beta^+)$ ,  $^{18}\text{O}(p, \alpha)$ , and  $^{15}\text{N}(\alpha, \gamma)^{19}\text{F}$ . Nuclear structure of  $^{19}\text{F}$  might be important for understanding production of the long-lived radioisotope  $^{18}\text{F}$  in novae and in heavy element production in x-ray bursts [3–7]. Here, the important reactions are  $^{18}\text{F}(p, \alpha)^{15}\text{O}$  and  $^{18}\text{F}(p, \gamma)^{19}\text{Ne}$ . These reactions proceed through the  $^{19}\text{Ne}$  nucleus. The authors of Refs. [3,4] noted that the needed information can be more easily obtained through studies of  $^{19}\text{F}$ , mirror to  $^{19}\text{Ne}$  nucleus.

Interest in the  $^{19}\text{F}$  nucleus is also supported by the general interest in the  $\alpha$ -cluster structure in atomic nuclei, well known in nearby  $^{20}\text{Ne}$  [8]. Recently it was shown [8,9] that the  $\alpha$ -cluster structure in odd-even  $^{21}\text{Ne}$  nucleus has striking

similarities to that of 4N nucleus  $^{20}\text{Ne}$ .  $^{19}\text{F}$  is important for comparison of the structures ( $^{17}\text{O} + \alpha$ ) and ( $^{15}\text{N} + \alpha$ ), where  $^{17}\text{O}$  has an extra nucleon and  $^{15}\text{N}$  has a hole relative to  $^{16}\text{O}$  core.

Recent decades saw some significant advances in microscopic understanding of clustering phenomena that stem from ideas of quantum configuration mixing involving shell-model-like wave functions with reaction channels. Building up on the ideas of the resonating group method [10–13], its algebraic extensions, and related generator coordinate methods [14] the new combined no-core shell model with resonating group method [15–17] have been gaining a foothold in modern studies. A recent development of the cluster center-of-mass boosting technique [18,21] that we utilize in this work has been a breakthrough method allowing us to extend clustering studies to a much broader scope of nuclei [20].  $\alpha$  clustering along with many other examples such as those discussed in Ref. [19] represents a curious manifestation of the near-threshold resonances with significant collectivization of spectroscopic strength towards the corresponding channels; this phenomenon is not fully understood.

In our previous works [8,9] we made first steps towards explanation of the properties of  $\alpha$ -cluster states in  $^{20,21}\text{Ne}$  using the recently developed configuration interaction

\*volya@phy.fsu.edu

TABLE I.  $^{19}\text{F}$  levels.

N	$J^\pi$	Ref. [28]		Ref. [3]		Ref. [22]		Ref. [4]		Ref. [5]		This work	
		$E'^a$ (MeV)	$\Gamma_\alpha^b$ (keV)	$E_x$ (MeV)	$\Gamma_\alpha$ (keV)	$E'$ (MeV)	$\Gamma_\alpha$ (keV)	$E'$ (MeV)	$\Gamma_\alpha$ (keV)	$E'$ (MeV)	$\Gamma_\alpha$ (keV)	$E'$ (MeV)	$\Gamma_\alpha$ (keV)
1	$1/2^+$	-	-	-	-	-	-	5.337	$1.3 \pm 0.5$	5.336	$2.51 \pm 0.10$	5.333	$1.4 \pm 0.4$
2	$3/2^+$	5.501	$4 \pm 1$	5.496	3.2	5.475	4	5.501	$4.7 \pm 1.6$	5.501	$6.0 \pm 0.3$	5.488	$4.85 \pm 0.5$
3	$5/2^+$	$6.282 \pm 2$	2.4	6.289	2.4	6.269	3	-	-	-	-	6.289	$2.30 \pm 0.5$
4	$7/2^+$	$6.330 \pm 2$	2.4	6.338	$3.6 \pm 0.4$	6.317	3	-	-	-	-	6.339	$3.30 \pm 0.4$
5	$1/2^-$	$6.429 \pm 8$	280	6.536	$245 \pm 6$	6.41	358	-	-	-	-	6.540	$220 \pm 40$
6	$1/2^-$	$6.989 \pm 3$	51	7.028	$96 \pm 6$	6.97	64	-	-	-	-	7.048	$150 \pm 35$

<sup>a</sup>Excitation energy in  $^{19}\text{F}$ .

<sup>b</sup> $\alpha$  width.

methods for clustering [20,21]. These theoretical developments are important both for better understanding of the clustering in atomic nuclei and for calculation of nuclear reaction induced by  $\alpha$  particles in stars. One has to realize that many nuclear reactions important for astrophysics cannot be tested in laboratories because of desperately small cross sections.

This work is a part of a series of several research papers targeting the many-body structure,  $\alpha$  clustering, and isospin symmetry near mass 20 region. In this paper we target the lowest  $\alpha$ -particle partial wave channels with  $\ell = 0$  and  $\ell = 1$  and the corresponding broad resonances  $1/2^-$ ,  $1/2^+$ , and  $3/2^+$  in  $^{19}\text{F}$ .

## II. EXPERIMENTAL DATA

Experimental information about broad  $\ell = 0$  and  $\ell = 1$  resonances of interest comes from our own experiment and from several previous studies and their reanalysis. The following section describes our work aimed to provide aggregate experimental data on the resonant parameters for the specific states of interest.

The only high-energy resolution, broad energy, and angle range experimental study of resonances in the  $\alpha + ^{15}\text{N}$  scattering was published over a half a century ago in Ref. [22]. The study covers a broad interval of the excitation energies in  $^{19}\text{F}$  from 5.37–8.33 MeV with energy resolution about 0.1%  $E$ . All of the angles at which the excitation functions were measured in Ref. [22], except  $169.1^\circ$ , correspond to zeros of Legendre polynomials. A contemporary  $R$  matrix analysis was made by authors of Ref. [3]. The authors of Ref. [3] were mainly motivated by the need for a more precise knowledge of the parameters of broad low spin resonances needed for calculations of the reaction rates in astrophysics. This analysis [3] also corrected multiple errors in the previous spins assignments for the levels with  $J = \ell \pm 1/2$ , which can be populated with the same orbital angular momentum of captured  $\alpha$  particle. Unfortunately, the authors of Ref. [3] could perform the analysis of the available digital data from Ref. [22] only for the  $169.1^\circ$  angle, and their analysis is restricted by 7.3 MeV excitation energy in  $^{19}\text{F}$ .

More recently two studies [4] and [5] of resonant  $\alpha + ^{15}\text{N}$  interaction in a narrow region of energy around 5.3 and 5.5 MeV of excitation in  $^{19}\text{F}$  were performed to obtain the total

widths and the partial  $\gamma$ -decay widths for  $1/2^+$  and  $3/2^+$  states in  $^{19}\text{F}$ . However, the results [4] and [5] on the widths of the states disagreed with each other well beyond the quoted uncertainties (see Table I).

In order to improve the data on low spin broad resonances close to the particle decay threshold in  $^{19}\text{F}$ , we reanalyzed the data [22] again. Differently from Ref. [3] we included in the analysis all data [22], at all measured angles, and in complete energy region; we also used a convolution of the  $R$  matrix calculations with experimental energy resolution.

The energy region covered by the measurements [22] did not include  $1/2^+$  resonance at 5.5 MeV. To explore this energy region and to bring the angular region of the measurement to  $180^\circ$  c.m. we performed measurements of the excitation functions for the  $\alpha + ^{15}\text{N}$  elastic scattering by the thick target inverse kinematic (TTIK) method [23,24]. In the TTIK technique the inverse kinematics is used, and the incoming ions are slow in a helium target gas. The light recoils,  $\alpha$  particles, are detected from a scattering event. These recoils hit a Si detector array located at forward angles while the beam ions are stopped in the gas, as  $\alpha$  particles have smaller energy losses than the beam ions. As a result of the slowing down of the beam the TTIK approach provides for a continuous excitation function. The measurements were made at DC-60 facilities at Nur Sultan (Kazakhstan) at  $^{15}\text{N}$  beam energy of 21 MeV, and all conditions were very similar to those described in Ref. [23]. Zero degrees measurements in the TTIK approach correspond to  $180^\circ$  c.m. The best energy resolution of the method (about 25 keV, [23]) is also reached at this angle. We found it to be 33 keV and tested it in a fit of well-known narrow  $5/2^+$  and  $7/2^+$  resonances in  $^{19}\text{F}$  (Ref. [23], see Table 1 and Fig. 2). Recently a study of the  $\alpha + ^{15}\text{N}$  elastic scattering using the TTIK method at higher excitation energy than in the present work was reported in Ref. [25], and we will analyze those results in a followup publication.

Figure 1 shows an  $R$  matrix fit of data of Ref. [22] at  $169.1^\circ$ . The  $R$  matrix calculations were performed with the code AZURE [26]. We obtained a reasonable fit to the data [22] at all angles and in the whole energy region of measurements [22] up to 8.3 MeV excitation energy. The full results of this analysis including over 50 resonances are published in Ref. [27].

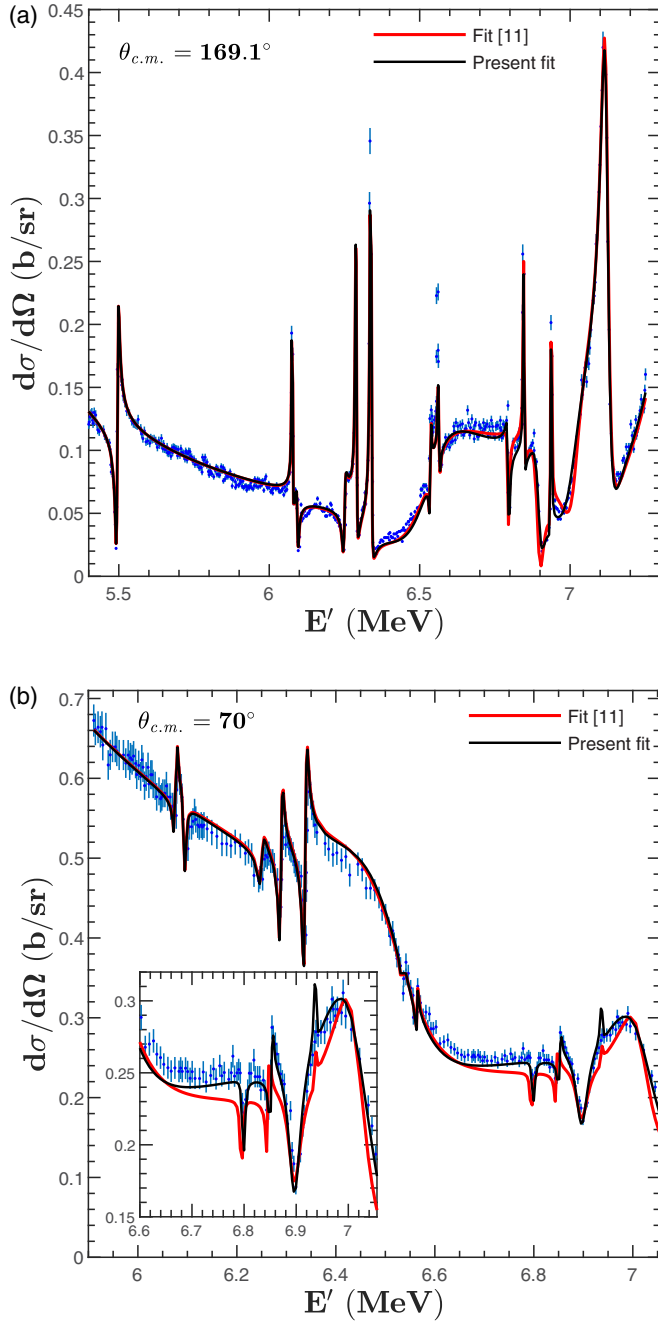


FIG. 1. (a)  $R$  matrix fit of the excitation functions for the  $\alpha + {}^{15}\text{N}$  elastic scattering [22] at  $169.1^\circ$  in comparison with the fit of the Ref. [3]; (b) the same for  $70^\circ$ . An inset highlights the difference between the present fit and the fit with parameters of Ref. [3].

Figure 1 was obtained using parameters for low spin states that are somewhat different from those in Ref. [3], see Table I, however, at  $169.1^\circ$  the difference is hardly noticeable. Usually, it is considered that the parameters of an  $R$  matrix analysis are most sensitive to the excitation functions measured at angles very close to  $180^\circ$ . This is because the potential scattering contribution decreases towards  $180^\circ$ , and the resonances are at their maximum. However, the  $\ell = 0$  resonances have an isotropic angular distribution, and can

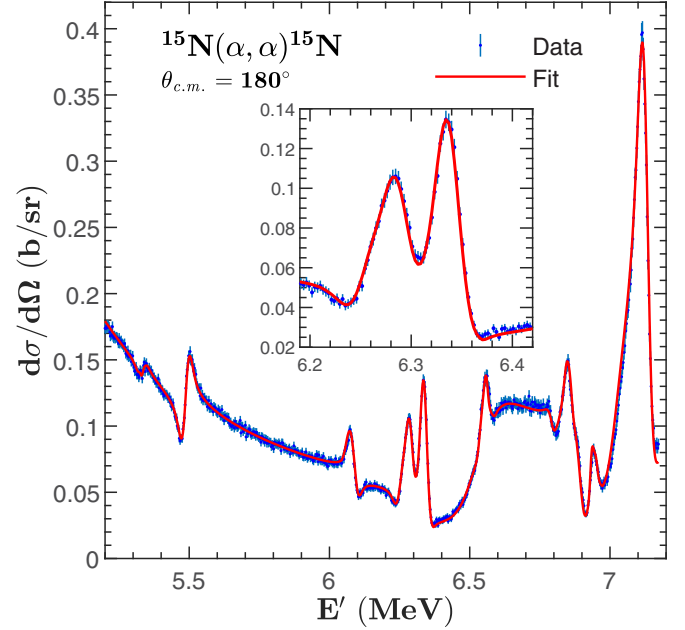


FIG. 2. The excitation function for  $\alpha + {}^{15}\text{N}$  elastic scattering. Inset:  $R$  matrix fit of the excitation function for  $\alpha + {}^{15}\text{N}$  elastic scattering in the region of  $5/2^+$  and  $7/2^+$  resonances, using convolution with experimental energy resolution of 33 keV.

manifest themselves as broad singularities at angles close to  $90^\circ$ , while the higher  $\ell$  resonances are weaker. Besides, it is worthwhile to note that the odd  $\ell$  resonances should be very weak in  $\alpha + {}^{15}\text{N}$  resonant scattering at  $90^\circ$ ; the odd Legendre polynomials that describe the scattering of spinless ions are equal to zero at this angle. We found that the fit with the parameters [3] deteriorates at angles close to  $70^\circ$ . As seen in Fig. 1, the modified parameters for  $\ell = 0$  resonances (Table I) provide a better description of the experimental data.

Figure 2 demonstrates an excitation function for  $\alpha + {}^{15}\text{N}$  elastic scattering at  $180^\circ$  obtained using the TTIK approach. An inset in Fig. 2 shows the excitation function in the region of the  $5/2^+$  ( $E' = 6.299$  MeV),  $7/2^+$  ( $E' = 6.339$  MeV) resonances using convolution with experimental resolution of 33 keV. Here and in tables  $E'$  refers to the energy above the  $\alpha$ -particle separation energy. Then we used the obtained energy resolution to fit the excitation function in the region of  $1/2^+$  and  $3/2^+$  resonances (Fig. 3). To test a dependence of the influence of the energy resolution on the evaluation of the widths  $1/2^+$  and  $3/2^+$  resonances, we varied it by 10%. It resulted in 0.1 keV variation of the evaluated widths.

Table I summarizes the results for the  $1/2^-$ ,  $1/2^+$ , and  $3/2^+$  resonances in question. Taking into account the uncertainties of the available data the total widths are:  $1/2^+$  ( $E' = 5.33$  MeV),  $\Gamma = 1.4 \pm 0.4$  keV, and  $3/2^+$  ( $E' = 5.50$  MeV);  $\Gamma = 5.4 \pm 0.4$  keV. Table II presents the reduced  $\alpha$ -particle widths of these states in  ${}^{19}\text{F}$  in comparison with the widths of the states with similar structure in  ${}^{20}\text{Ne}$  [8]. It is evident from Table II that the states with a similar core ( ${}^{15}\text{N}$  or  ${}^{16}\text{O}$ )+ $\alpha$ -particle structure appear at the energies close to the alpha particle decay thresholds in  ${}^{19}\text{F}$  and  ${}^{20}\text{Ne}$ .

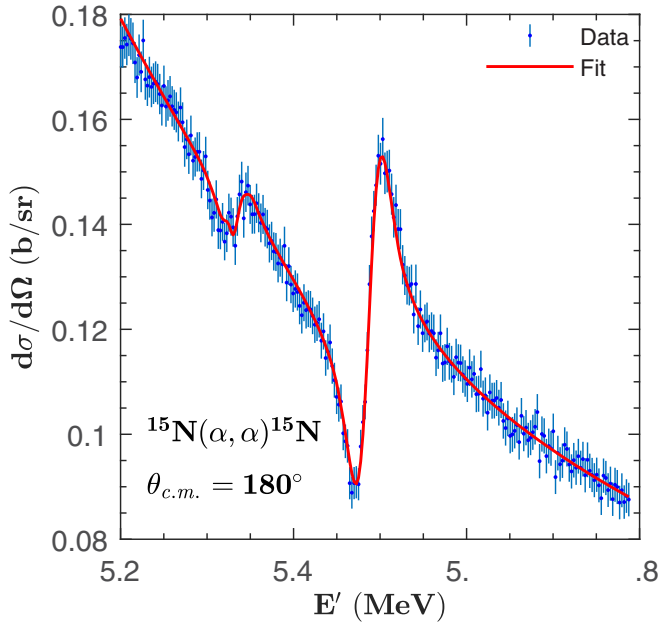


FIG. 3.  $R$  matrix fit of the region of  $1/2^+$  (5.3 MeV) and  $3/2^+$  (5.5 MeV) levels in  $^{19}\text{F}$  measured by TTIK method. The level parameters are given in Table I.

### III. THEORY

Despite the success of the many-body techniques that stem from *ab initio* principles full microscopic description of spectra of sufficiently large nuclei is difficult unless effective interactions are considered, which are at the core of the traditional shell model [29]. Recently a new FSU interaction Hamiltonian has been developed [30–32] where cross-shell matrix elements between  $p$ ,  $sd$ , and  $fp$  shells have been determined using the latest data on masses and energies of intruder states. The FSU interaction Hamiltonian is among the most broad in its region of applicability covering a valence space from the  $s$  shell to  $fp$  shell, it has been demonstrated to be remarkably accurate, and works well for exotic states with multiparticle cross shell excitations that were not a part of the fit, see Refs. [30–32]. The FSU effective interaction has not yet been explored in any clustering studies but we use it in this work because given its nature it seems to bear the most

TABLE II.  $\alpha$ -particle widths of the states with similar structure in  $^{19}\text{F}$  and  $^{20}\text{Ne}$  [9].

$^{20}\text{Ne}$				$^{19}\text{F}$			
$J^\pi$	$E'^a$ (MeV)	$\Gamma_\alpha$ (keV)	$\gamma_\alpha^b$	$J^\pi$	$E'$ (MeV)	$\Gamma_\alpha$ (keV)	$\gamma_\alpha$
$1^-$	1.1	0.028	1.4	$1/2^+$	1.3	1.4	0.65
-	-	-	-	$3/2^+$	1.5	5.4	0.88
$0^+$	2.0	19	0.47	$1/2^-$	2.4	220	0.51
$0^+$	2.5	3.4	0.17	$1/2^-$	3.0	150	0.12

<sup>a</sup> $E'$  is the excitation energy relative to the  $\alpha$ -particle decay threshold (4.7 MeV for  $^{20}\text{Ne}$  and 4.0 MeV for  $^{19}\text{F}$ ).

<sup>b</sup>Reduced  $\alpha$  width of the level.

TABLE III. Lowest states coupled to  $\ell = 0$  channel. Top part of the table shows states in  $^{20}\text{Ne}$  for the  $^{16}\text{O} + \alpha$  reaction and bottom part corresponds to  $^{19}\text{F}$  and  $^{15}\text{N} + \alpha$  reaction. Columns identify state, theoretical excitation energy, number of nodes in the  $\alpha$  channel, experimental energy, experimental  $\alpha$  reduced width, experimental proton spectroscopic factor, and theoretical proton spectroscopic factor. The labels in the second row “th” or “expt” refer to results coming from theory and experiment, respectively. Correspondence between data from theory and experiment is not a firm assignment, see discussion in text. The states assessed in this work are marked with \*.

$J_i^\pi$	$E$ (MeV)	$n$	$\text{SF}_\alpha$	$E$ (MeV)	$\gamma_\alpha$	$\text{SF}_p$	$\text{SF}_p$
th	th	th	th	expt	expt	expt	th
$0_1^+$	0	4	0.755	0			
$0_2^+$	6.698	4	0.143	6.725	0.47		
$0_3^+$	7.547	5	0.007	7.191	0.017		
$0_4^+$	10.121	6	0	8.7	broad		
$0_5^+$	11.885	5	0.093				
$0_6^+$	11.908	4	0.002				
$0_7^+$	12.160	5	0.002				
$0_8^+$	13.521	5	0.246				
$1/2_1^-$	0.468	4	0.706	0.110		0.24	0
$1/2_2^-$	6.900	4	0.020	(6.095)		0.12	0.04
$1/2_3^-$	7.092	4	0.041	7.048*	0.12		0.02
$1/2_4^-$	7.292	5	0.006	7.702			-
$1/2_5^-$	7.856	4	0.101	6.540*	0.53		0.11
$1/2_6^-$	8.761	4	0.003				0.02

potential for helping to understand the physics of clustering in light-to-medium mass nuclei.

The FSU interaction describes well the  $^{19}\text{F}$  spectrum, there is a good correspondence, within a few hundreds of keV, between the shell model results and experimental data. For the most part this agreement is to be expected because FSU interaction is built using well-established effective matrix elements that have been fitted and are known to work well in this mass region, see Refs. [30–32] and references therein. Full analysis of the large number of states in  $^{19}\text{F}$  coming from the shell model calculation will be reported elsewhere along with a complete experimental  $R$  matrix analysis. Our goal here is to complement experimental evaluations reported in the previous section and to look at the  $\alpha + \text{core}$  dynamics in the channels with low angular momentum. Due to the small centrifugal barrier these are the situations where decays into  $\alpha$  channels are strong, and the presence of broad resonances has significant effect on the many-body structure. As mentioned earlier these broad resonances have been problematic within previous theoretical studies and thus are of special interest. Thus, we limit consideration to the partial waves with  $\ell = 0$  and  $\ell = 1$ . Also, we concentrate on the states above the threshold.  $\alpha$ -separation energy in  $^{19}\text{F}$  is at 4.013 MeV so states above that would not be visible in  $\alpha$  scattering experiments.  $\alpha$ -separation energy in  $^{20}\text{Ne}$  is 4.7299 MeV.

The relevant shell model predictions obtained using FSU interaction and using the techniques of Ref. [20] are compared with experimental data on clustering in the following tables: III for  $\ell = 0$  and in IV for  $\ell = 1$ .

TABLE IV. Same as Table III but for  $\ell = 1$  channel. The  $1/2^+$  and  $3/2^+$  spin-orbit partner states are listed separately.

$J_i^\pi$ th	$E(\text{MeV})$ th	$n$ th	$\text{SF}_\alpha$ th	$E(\text{MeV})$ expt	$\gamma_\alpha$ expt	$\text{SF}_p$ expt	$\text{SF}_p$ th
$1_1^-$	6.982	4	0.381	5.79	1.4		
$1_2^-$	7.918	4	0.379	8.708			
$1_3^-$	8.957	4	0.010	8.854			
$1_4^-$	10.529	4	0.005				
$1/2_1^+$	0.000	3	0.874	0.000		0.42	0.76
$1/2_2^+$	6.060	4	0.311	5.333*	1.16		-
$1/2_3^+$	6.212	3	0.034	6.255		0.19	0.13
$1/2_4^+$	7.199	4	0.027	5.938		0.014	-
$1/2_5^+$	8.801	3	0.003	8.135		0.156	0.50
$3/2_1^+$	1.770	3	0.672	1.554		1.01	0.79
$3/2_2^+$	4.877	4	0.003	3.908			-
$3/2_3^+$	6.819	3	0.019	6.497		0.133	0.04
$3/2_4^+$	6.937	4	0.633	5.488*	0.98		-
$3/2_5^+$	7.080	3	0.136	6.528			0.01
$3/2_6^+$	7.847	4	0.040	7.262			-

Our previous theoretical efforts [8,9] that used fully mixed calculations within two oscillator shells were successful for states mostly within  $0\hbar\omega$  excitation, but some positions of states in the spectra and clustering collectivization were not reproduced for the negative parity (mainly  $1\hbar\omega$ ) states and for states of both parities dominated by higher cross-shell excitations. Yet, this and multiple other experiments indicate that at the microscopic level strong clustering strength, which cumulatively exceeds the single-particle Wigner limit comes from different  $\alpha$  channels. The channels can be identified with a different number of nodes in the relative  $\alpha$  plus core wave function. This suggests collectivization toward clustering channel within each set of states of a given harmonic oscillator quanta of excitation  $\hbar\omega$ . A recently published study of  $^{20}\text{Ne}$  [33], which produces similar results and highlights the effectiveness of the algebraic techniques built around harmonic oscillator shell structure supports this idea. Thus, in this work we approach with different theoretical strategy and use the FSU shell model interaction that is built with the particle-hole excitation hierarchy in mind. This helps us to understand the clustering collectivization and to have a clear harmonic oscillator based identification of clustering channels using the number of oscillator quanta. Effects of many-body mixing and interaction through the continuum are to be explored later.

The experimental results discussed in the previous section point to a close relation between low-lying  $\alpha$ -cluster levels in  $^{20}\text{Ne}$  and  $^{19}\text{F}$ . Considering this, let us start with the lowest  $J = 0$  states in  $^{20}\text{Ne}$  and examine them in terms of  $^{16}\text{O} + \alpha$  in  $\ell = 0$  channel, see Table III. Within the harmonic oscillator picture the lowest allowed configuration involves placing the four nucleons onto  $sd$  shell. If we assume that in the same basis the  $\alpha$  particle has no intrinsic harmonic oscillator excitations then all eight quanta must be carried out by the relative  $^{16}\text{O} + \alpha$  motion, which amounts to the relative wave function having  $n = 4$  nodes. This number is listed in the third column of Table III. In our notations the total number of oscillator quanta is given by  $2n + \ell$ , where  $n$  is the number of nodes

in the radial wave function not counting the origin. Details of the oscillator algebra can be found in many textbooks, see for example Ref. [34]. The excitation energy of the first excited  $0^+$  state at 6.7 MeV agrees well with experiment, see Table II  $E' = 2.0$  MeV, this state is also clustered with spectroscopic factor  $\text{SF}_\alpha = 0.14$ . Here we define spectroscopic factor as an overlap of the normalized  $\alpha$ -channel wave function with the state of interest, squared, for details see Ref. [20]. Without mixing of particle-hole configurations the sum of all spectroscopic factors for a given channel is normalized to unity (excluding spin degeneracy). The magnitude of the SF is expected to be roughly proportional to the reduced width  $\gamma_\alpha$  obtained from experiment as the ratio of observed decay width to the width obtained for a resonance at the same energy in the potential model. Both lowest states are  $sd$  states coupling to the  $\alpha$ -channel wave function with  $n = 4$ . The next  $0_3^+$  state predicted at 7.5 MeV is likely a counterpart to the next known state at 7.19 MeV (listed in Table II  $E' = 2.7$  MeV). This state is a  $2\hbar\omega$  state dominated by the two particle-hole excitation of nucleons from  $p$  to  $sd$  shells. This is an  $n = 5$  node state with respect to the clustering channel, but in agreement with experiment this state has a much smaller  $\alpha$  SF. The main clustering strength for  $\alpha$  scattering in  $n = 5$  channel appears in our theoretical model at higher energy, around 13.5 MeV. In addition the shell model predicts  $4\hbar\omega$  state  $0^+$  state at 10 MeV ( $n = 6$ ). Configuration mixing and coupling to the continuum suggest these states as candidates for explaining a broad  $\alpha$  resonance seen in experiments.

It is instructive to compare these results with those reported in Ref. [9]. The previous calculations were done using several older and more restrictive theoretical models, the  $n = 4$  channel results ( $0\hbar\omega$  valence space) agree well with those from USDB Hamiltonian [35] restricted to  $sd$  shell, the  $2\hbar\omega$  states coupled to  $n = 5$  channel emerge from consideration of  $p$ - $sd$  space with Hamiltonian from Ref. [36]. The  $p$ - $sd$  Hamiltonian used in Ref. [9] allowed for  $\hbar\omega$  mixing but the valence space limitation limits its applicability to  $n = 4$  and  $n = 5$ . The  $4\hbar\omega$  excitations are not reasonable to discuss without the  $fp$  oscillator shell. It appears that the mixing between  $0\hbar\omega$  and  $2\hbar\omega$  in the Hamiltonian from Ref. [36] is excessive, giving a  $0_3^+$  state a much larger  $\alpha$  SF. Both the previous work and these results do not reproduce the broad  $0_4^+$  state but the emergence of the  $4\hbar\omega$  state in this study, which couples to the  $\alpha$  channel with  $n = 6$  nodes, offers a way to explain the appearance of significant new  $\alpha$  strength coming with a new  $\alpha$  channel that has  $n = 6$  nodes in the  $\alpha$ -core relative wave function. It is likely that configuration mixing and coupling through the continuum redistribute and lower this strength, making  $0_4^+$  very broad. Further theoretical efforts, larger valence space, and more elaborate models are needed to understand the lowering of the  $\alpha$  strength.

Let us now turn to an analogous situation in  $^{15}\text{N} + \alpha$  reaction. Because of the  $0p_{1/2}$  proton hole in  $^{15}\text{N}$  the  $\ell = 0$  channel with  $n = 4$  nodes would couple to  $1/2^-$   $1\hbar\omega$  states in  $^{19}\text{F}$ . Roughly speaking,  $\alpha$  particle in this relative motion adds eight oscillator quanta to the system by placing four nucleons on the  $sd$  shell. See bottom part of Table III. The lowest  $1/2^-$  state predicted by the shell model at 0.47 MeV appears to correspond to this situation and has a large  $\alpha$  SF. The

experimental counterpart at 0.11 MeV of excitation is below the  $\alpha$  threshold for direct scattering. Above that, both theory and experiment have a series of  $1/2^-$  states starting at about 6.5 MeV of excitation. The state seen at 6.54 MeV with reduced width of 0.53 is a likely clustering analog to  $0_2^+$  in  $^{20}\text{Ne}$ . In theory this state appears at 7.8 MeV and absorbs the remaining strength for  $\alpha$  in  $\ell = 0$   $n = 4$  channel. The theoretical  $\alpha$  SF's 0.14 for  $^{20}\text{Ne}$  and 0.1  $^{19}\text{F}$  are similar. In our model we do not consider any mixing between different  $\hbar\omega$  states, of course, this mixing should be present, but in nearly spherical nuclei and without other significant collective dynamics we expect this mixing to be small. The lack of mixing would suggest that particle decays from states with larger number of excitation quanta would be blocked. This seems to be supported by experiments, the spin-orbit analog states  $1/2^+$  at 5.333 MeV and  $3/2^+$  at 5.488 MeV for  $\ell = 1$   $n = 4$  channel, discussed in the following text, are not seen in  $^{18}\text{O}(d, n)$  reactions [37] although other states of the same spin and parity below and above in excitation energy are seen, see Table IV. In our model the  $1/2_4^-$  state that appears at 7.292 MeV of excitation is  $3\hbar\omega$  state that couples to  $n = 5$  node  $\alpha$ -channel wave function. The proton decay of this state to the ground state is suppressed because it would require proton to carry out five oscillator excitation quanta and effectively decay from  $2p_{1/2}$  orbit of the  $pfh$  oscillator shell, which is very high. The selection rules related to the number of oscillator quanta are helpful in discussions of other transitions. The  $1/2_4^-$  state in  $^{19}\text{F}$  could be associated with  $0_3^+$  in  $^{20}\text{Ne}$ , which is of  $2\hbar\omega$  type and thus both states would couple to  $n = 5$   $\ell = 0$   $\alpha$  channel. However, both states have small  $\text{SF}_\alpha$  to this channel (0.007 in  $^{20}\text{Ne}$  and 0.0055 in  $^{19}\text{F}$ ) so these are not cluster states.

The  $1/2^-$  state at 7.0 MeV observed in this work has a reduced width of 0.12 and therefore is unlikely to be  $3\hbar\omega$ . The shell model predicts several other states around 7 MeV of excitation that capture enough  $\alpha$  strength in the  $n = 4$  channel. The two states at 7.048 MeV and 6.540 observed in experiments are likely the  $1/2_3^-$  and  $1/2_5^-$  states that are both coupled to  $n = 4$   $\alpha$  channel. These states being near in the spectrum, of the same spin-parity, and having the same number of oscillator quanta obviously mix and share the  $\alpha$  strength. Based on the  $\alpha$  channel coupling strength we identify 6.540 MeV state with shell model one  $1/2_5^-$  at 7.856, but this identification is subjective. In stars this state can provide a path for generation of  $^{19}\text{F}$  via  $(\alpha, \gamma)$  process [3]. Experimentally the  $\gamma$  width is not known but theory predicts two main  $\gamma$ -decay branches:  $E1$  to the  $1/2^+$  ground state width 0.14 eV [ $B(E1) = 0.0011$  W.u.] and  $M1$  to the first excited  $1/2_1^-$  state with width 0.06 eV [ $B(M1) = 0.012$  W.u.]

It is interesting to note that no counterpart for the broad  $0^+$  state at 8.7 MeV has yet been seen in  $^{19}\text{F}$ , which suggests that the structure of this state and its strong coupling to continuum is indeed influenced by special circumstances. This question calls for a separate discussion and we plan to address it in our future work.

In the  $\ell = 1$  channel there is a broad  $1^-$  state observed at 5.79 MeV in  $^{20}\text{Ne}$ . In theory there are two states predicted at 6.9 and 7.9 MeV that are strongly coupled and share nearly full  $\alpha$  strength in  $\ell = 1$   $n = 4$  channel. Strong coupling to a decay channel is known to cause a superradiance mechanism

in overlapping resonances leading to full decay width being absorbed by one of the states [38,39]. Thus the superradiant  $1^-$  is likely the state seen in experiments and redistribution of the width that this theory is unable to describe is not surprising.

The comparison between  $^{15}\text{N} + \alpha$  and  $^{16}\text{O} + \alpha$  is more interesting in  $\ell = 1$  because negative parity of the relative motion allows both  $n = 3$  channel  $^{15}\text{N} + \alpha$  while this channel is Pauli blocked for  $^{16}\text{O} + \alpha$ . Effectively a proton hole in  $^{15}\text{N}$  can be occupied by one of the protons from an  $\alpha$  particle in  $^{15}\text{N} + \alpha$ , which is not possible in the case of  $^{16}\text{O}$ . Difficulty of the previously used theoretical methods to describe odd-parity  $\alpha$  channels in  $^{20}\text{Ne}$  adds relevance to this comparison.

Let us discuss the  $n = 4$ ,  $\ell = 1$  channel. The scattering of  $^{15}\text{N} + \alpha$  in this channel would populate  $2\hbar\omega$  states in  $^{19}\text{F}$ . Indeed, the second excited  $1/2_2^+$  state predicted at 6.06 MeV and  $3/2_4^+$  predicted at 6.94 MeV both have this structure and are strongly coupled to this  $\alpha$  channel. This is consistent with experiments where these states appear at 5.33 MeV ( $1/2^+$ ) and 5.49 MeV ( $3/2^+$ ). The  $0\hbar\omega$  states should have an appreciable single-particle spectroscopic factor, which can be measured in the  $^{18}\text{O}(d, n)$  reaction. The correlation between the calculations and the experimental results is evident in Table IV.

Our theoretical approach is certainly not perfect; mixing of states and involvement of the scattering continuum using more advanced theory such as continuum shell model [40–42] is yet to be done. However, the fact that strongly clustered  $1/2^+$  and  $3/2^+$  are spin-orbit partners in the  $n = 4$ ,  $\ell = 1$  channel is transparent; this channel and the corresponding broad  $1^-$  state are well known in  $^{16}\text{O} + \alpha$  reaction. In  $^{19}\text{F}$  the  $1/2^+$  and  $3/2^+$  clustering states in  $n = 4$   $\ell = 1$  channel are  $2\hbar\omega$  states, which should suppress their particle spectroscopic factors and may have an effect on their  $\gamma$  decays. Assessing this spectroscopic information from experiment, exploration of the channel mixing via resonating group method, and study of configuration mixing related to channel coupling and continuum are of interest.

#### IV. CONCLUSIONS

In this work we explore  $^{19}\text{F}$  and its structure as  $^{15}\text{N} + \alpha$  targeting exclusively  $\ell = 0$  and 1 partial waves. We determine parameters of several resonances populated in the  $^{15}\text{N}$  ( $\alpha, \alpha$ ) elastic scattering. The  $^{19}\text{F}$  plays an important role in astrophysics and its structure is central for the development of theoretical understanding of the nuclear many-body problem; of clustering and interplay between structure and reactions, in particular.

As compared to oxygen chain, an extra proton in fluorine isotopes makes a huge structural difference, changing the mean-field shape, pairing properties, and extending the neutron drip line much further in the mass number [42]. We explore this through the comparison between  $^{15}\text{N} + \alpha$  and  $^{16}\text{O} + \alpha$  reactions and correspondingly  $\alpha$  structure of states in  $^{19}\text{F}$  and  $^{20}\text{Ne}$ .

In this work we concentrate on the channels with relative motion in the lowest partial waves with  $\ell = 0$  and  $\ell = 1$ , which couple to the low-lying states and due to the small

centrifugal barrier are most impactful in structure-reactions physics and in astrophysics. We find that the clustering structure prevails; for  $\ell = 0$  we identify a 6.540 MeV  $1/2^-$  state that appears to be a counterpart of 6.725 MeV state in  $^{20}\text{Ne}$  with  $\alpha$  moving relative to the core in a state with  $n = 4$  nodes in the radial wave function. The situation with  $\ell = 1$  is interesting, here in  $^{20}\text{Ne}$  the  $1^-$   $\alpha$  strength that appears in 5.79 MeV state comes in the scattering channel  $^{16}\text{O} + \alpha$  with  $n = 4$  nodes; in  $^{19}\text{F}$  lowest states are coupled to a different  $n = 3$  channel, which is not blocked by the Pauli principle, and yet in this work we were able to identify cluster resonant states in  $^{19}\text{F}$  representing  $^{15}\text{N} + \alpha$  relative motion with  $n = 4$ . The states in  $^{19}\text{F}$ ,  $1/2^+$  at 5.333 MeV and  $3/2^+$  at 5.488 MeV, are spin-orbit partners coupling  $1/2^-$  ground state of  $^{15}\text{N}$  with orbital  $\ell = 1$  motion of  $\alpha$ .

Thanks to a combined experimental and theoretical research targeting only specific broad states, we were able to make a substantial progress in understanding of clustering. We take advantage of a new phenomenological shell model Hamiltonian [30–32] that has been developed to study cross-shell particle-hole excitations. While particle-hole hierarchy in the theoretical approach may seem like a disadvantage in this work it played a crucial role in identifying clustering channels, allowing us to determine origins of seemingly excessive clustering strength observed in experiments. In particular, a clear separation between scattering states with different number of radial nodes allows us to cleanly establish spin-orbit partner states in  $^{15}\text{N} + \alpha$ ,  $\ell = 1$  channel, while accounting for all other resonances and their strengths in  $^{19}\text{F}$ . This resolves many issues encountered in previous

works [8,9,43]. Prevalence of clustering and the emergence of strongly clustered states from a microscopical perspective appears to represent collectivization of states with a certain number of oscillator cross-shell excitations. The reasons for this collectivization, its enhanced strength near thresholds, and apparent lack of mixing of states with different particle-hole nature are yet to be studied. The particle-hole hierarchy also suggests suppression of particle and electromagnetic transitions and offers avenues for experimental assessment of channel mixing and evaluation of continuum effects. This suppression may play an important role in astrophysical process and should be considered when going beyond a purely statistical treatment of reactions. For the first time we were able to discuss the spin-orbit interaction for clusters from a microscopic perspective and compare it with observations; this interaction appears to be very weak and due to many-body complexity it is impossible to separate any systematic strength that is not consistent with zero.

## ACKNOWLEDGMENTS

This material is based upon work supported by the U.S. Department of Energy Office of Science, Office of Nuclear Physics under Awards No. DE-SC0009883 and No. DE-FG02-93ER40773. Authors also acknowledge SSH2020014 project funded by Nazarbayev University, the Ministry of Education and Science of the Republic of Kazakhstan (Program No. BR05236454) and young scientists research Grant No. AP08052268.

- 
- [1] I. Indelicato, M. La Cognata, C. Spitaleri, V. Burjan, S. Cherubini, M. Gulino, S. Hayakawa, Z. Hons, V. Kroha, L. Lamia, M. Mazzocco, J. Mrazek, R. G. Pizzone, S. Romano, E. Strano, D. Torresi, and A. Tumino, *Astrophys. J.* **845**, 19 (2017).
- [2] H. Jönsson, N. Ryde, E. Spitoni, F. Matteucci, K. Cunha, V. Smith, K. Hinkle, and M. Schultheis, *Astrophys. J.* **835**, 50 (2017).
- [3] D. W. Bardayan, R. L. Kozub, and M. S. Smith, *Phys. Rev. C* **71**, 018801 (2005).
- [4] S. Wilmes, V. Wilmes, G. Staudt, P. Mohr, and J. W. Hammer, *Phys. Rev. C* **66**, 065802 (2002).
- [5] A. Di Leva, G. Imbriani, R. Buompane, L. Gialanella, A. Best, S. Cristallo, M. De Cesare, A. D’Onofrio, J. G. Duarte, L. R. Gasques, L. Morales-Gallegos, A. Pezzella, G. Porzio, D. Rapagnani, V. Roca, M. Romoli, D. Schürmann, O. Straniero, and F. Terrasi, *Phys. Rev. C* **95**, 045803 (2017).
- [6] H. T. Fortune, *Phys. Rev. C* **102**, 024333 (2020).
- [7] H. T. Fortune and R. Sherr, *Phys. Rev. C* **73**, 024302 (2006).
- [8] A. K. Nurmukhanbetova, V. Z. Goldberg, D. K. Nauruzbayev, M. S. Golovkov, and A. Volya, *Phys. Rev. C* **100**, 062802(R) (2019).
- [9] D. K. Nauruzbayev, V. Z. Goldberg, A. K. Nurmukhanbetova, M. S. Golovkov, A. Volya, G. V. Rogachev, and R. E. Tribble, *Phys. Rev. C* **96**, 014322 (2017).
- [10] A. Wheeler, *Phys. Rev.* **52**, 1107 (1937).
- [11] K. Wildermuth and Y. C. Tang, *A Unified Theory of the Nucleus* (Vieweg, Germany, 1977).
- [12] Y. C. Tang, M. LeMere, and D. R. Thompson, *Phys. Rep.* **47**, 167 (1978).
- [13] T. Fliessbach and H. Walliser, *Nucl. Phys. A* **377**, 84 (1982).
- [14] P. Descouvemont and D. Baye, *Phys. Lett. B* **505**, 71 (2001).
- [15] S. Quaglioni and P. Navrátil, *Phys. Rev. C* **79**, 044606 (2009).
- [16] P. Navrátil and S. Quaglioni, *Phys. Rev. Lett.* **108**, 042503 (2012).
- [17] P. Navrátil, S. Quaglioni, G. Hupin, and C. Romero-Redondo, and A. Calci, *Phys. Scr.* **91**, 053002 (2016).
- [18] K. Kravvaris and A. Volya, *J. Phys. Conf. Ser.* **863**, 012016 (2017).
- [19] J. Okołowicz, M. Płoszajczak, and W. Nazarewicz, *Phys. Rev. Lett.* **124**, 042502 (2020).
- [20] K. Kravvaris and A. Volya, *Phys. Rev. C* **100**, 034321 (2019).
- [21] K. Kravvaris and A. Volya, *Phys. Rev. Lett.* **119**, 062501 (2017).
- [22] H. Smotrich, K. W. Jones, L. C. McDermott, and R. E. Benenson, *Phys. Rev.* **122**, 232 (1961).
- [23] K. P. Artemov, O. P. Belyanin, A. L. Vetoshkin, R. Wolskj, M. S. Golovkov, V. Z. Goldberg, M. Madeja, V. V. Pankratov, I. N. Serikov, V. A. Timofeev, V. N. Shadrin, J. Szmider, *Soviet J. Nucl. Phys.*, **52**, 408 (1990).
- [24] A. K. Nurmukhanbetova, V. Z. Goldberg, D. K. Nauruzbayev, G. V. Rogachev, M. S. Golovkov, N. A. Mynbayev, S.

- Artemov, A. Karakhodjaev, K. Kuterbekov, A. Rakhymzhanov, Z. Berdibek, I. Ivanov, A. Tikhonov, V. I. Zherebchevsky, S. Y. Torilov, and R. E. Tribble, *NIM A* **847**, 125 (2017).
- [25] M. La Cognata, M. Fisichella, A. DiPietro, P. Figuera, V. Z. Goldberg, S. Cherubini, J. P. Fernández Garcia, M. Gulino, L. Lamia, D. Lattuada, M. Lattuada, R. G. Pizzone, G. G. Rapisarda, S. Romano, R. Spartá, C. Spitaleri, D. Torresi, A. Tumino, and M. Zadro, *Phys. Rev. C* **99**, 034301 (2019).
- [26] Azure r-matrix program, <https://azure.nd.edu>.
- [27] V. Z. Goldberg, A. K. Nurmukhanbetova, A. Volya, D. K. Nauruzbayev, G. E. Serikbayeva, and G. V. Rogachev, *Phys. Rev. C* **105**, 014615 (2022).
- [28] D. R. Tilley, H. R. Weller, C. M. Cheves, and R. M. Chasteler, *Nucl. Phys. A* **595**, 1 (1995).
- [29] B. A. Brown, *Prog. Part. Nucl. Phys.* **47**, 517 (2001).
- [30] R. S. Lubna, K. Kravvaris, S. L. Tabor, V. Tripathi, E. Rubino, and A. Volya, *Phys. Rev. Research* **2**, 043342 (2020).
- [31] R. S. Lubna, K. Kravvaris, S. L. Tabor, Vandana Tripathi, A. Volya, E. Rubino, J. M. Allmond, B. Abromeit, L. T. Baby, and T. C. Hensley, *Phys. Rev. C* **100**, 034308 (2019).
- [32] R. S. Lubna, PhD. thesis, Florida State University, 2019.
- [33] A. C. Dreyfuss, K. D. Launey, J. E. Escher, G. H. Sargsyan, R. B. Baker, T. Dytrych, and J. P. Draayer, *Phys. Rev. C* **102**, 044608 (2020).
- [34] M. Moshinsky and Y. F. Smirnov, *The Harmonic Oscillator in Modern Physics*, Contemporary Concepts, Physics Vol. 9 (Harwood Academic, Amsterdam, 1996).
- [35] B. A. Brown and W. A. Richter, *Phys. Rev. C* **74**, 034315, (2006).
- [36] Y. Utsuno and S. Chiba, *Phys. Rev. C* **83**, 021301(R), 2011.
- [37] A. Terakawa, H. Orihara, M. Oura, M. Hosaka, H. Suzuki, K. Kumagai, Y. Kikuchi, T. Tohei, T. Nakagawa, J. Takamatsu, A. Narita, K. Hosomi, K. Ishii, G.C. Jon, K. Miura, and H. Ohnuma, *Phys. Rev. C* **66**, 064313 (2002).
- [38] K. Kravvaris and A. Volya, in *Nuclei and Mesoscopic Physics 2017*, edited by P. Danielewicz and V. Zelevinsky, AIP Conf. Proc. No. 19112 (AIP, New York, 2017), p. 020010.
- [39] N. Auerbach and V. Zelevinsky, *Rep. Prog. Phys.* **74**, 106301 (2011).
- [40] A. Volya and V. Zelevinsky, *Phys. Rev. C* **74**, 064314 (2006).
- [41] A. Volya and V. Zelevinsky, *Phys. Rev. Lett.* **94**, 052501 (2005).
- [42] D. S. Ahn, N. Fukuda, H. Geissel, N. Inabe, N. Iwasa, T. Kubo, K. Kusaka, D. J. Morrissey, D. Murai, T. Nakamura, M. Ohtake, H. Otsu, H. Sato, B. M. Sherrill, Y. Shimizu, H. Suzuki, H. Takeda, O. B. Tarasov, H. Ueno, Y. Yanagisawa, and K. Yoshida, *Phys. Rev. Lett.* **123**, 212501 (2019).
- [43] M. L. Avila, G. V. Rogachev, V. Z. Goldberg, E. D. Johnson, K. W. Kemper, Yu. M. Tchuvil'sky, and A. Volya, *Phys. Rev. C* **90**, 024327, (2014).